

Article

Switching Modes of Mixing Due to an Adjustable Gap in a Continuous-Flow Microreactor

Dmitry Bratsun *  and Ramil Siraev

Department of Applied Physics, Perm National Research Polytechnic University, 14990 Perm, Russia; RRSiraev@pstu.ru

* Correspondence: DABratsun@pstu.ru; Tel.: +7-342-239-14-14

Received: 30 November 2019; Accepted: 18 December 2019; Published: 23 December 2019



Abstract: Microreactors are an important development in chemical engineering since the pharmaceutical industry needs flexible production rather than a large amount of product yield. The size of the microreactor may be so small that it requires the development of non-mechanical methods for reagent mixing. In this paper, we propose the design of a continuous-flow microreactor in the form of a narrow cell with a variable gap. By tuning the gap width in time and space, one can control the reaction rate and regulate the product yield. We show that the governing equation for the fluid flow can be reduced to the Darcy equation with permeability varying in space and time. As a test reaction, we consider the neutralization of nitric acid with sodium hydroxide resulting in the solutal convection in the presence of gravity. We show numerically that the prototyping spatially-distributed relief of the reactor walls can successfully separate the incoming and outgoing flows of reagents, control the mixing intensity, increase or decrease the product yield. We demonstrate also the dynamic control of the reactor efficiency via real-time local changes in the gap width.

Keywords: continuous-flow reactor; convective mixing; Hele-Shaw cell with a variable gap

1. Introduction

The development of chemical technologies dates back to the 1950s and 60s. The first theoretical description of heat and mass transfer in the reactors was given within physicochemical hydrodynamics [1,2]. Further development of technologies based on these principles is described in [3]. The traditional chemical production, as a rule, is carried out in the discontinuous stirred reactor (or batch reactor (BR)). In industry, discontinuous operations are well suited for rather complex reactions and allow one to drive the process by controlling the temperature [4]. In contrast to the BR, the continuous operations traditionally were typical for large productions (for example, in the oil and gas industry) based on a more simple chemistry [4]. Significant changes in this area occurred in the early 2000s when the new technologies penetrated an organic synthesis [5–7]. Since the pharmaceutical production needs more flexibility in reconfiguring the synthesis system rather than large product volume, the process has been developing towards the design of increasingly miniature reactors or microreactors [6,7]. The advantages of this new reactor type, the continuous-flow microreactor (hereinafter, CFMR) against the BR are: high productivity due to the elimination of loading-unloading stage; the stable consumption of reagents and energy due to the small reactor zone; the replication of the production line to increase product yield, just to mention a few. Consequently, numerous studies have been published in recent years detailing the beneficial outcome of continuous-flow chemistry applied to single or indeed multi-step syntheses of target compounds on various reaction schemes and spatial scales [8–11].

To mix the reagents in the CFMR, two basic physical principles can be used: diffusion and/or convection. When using the diffusion as the main mixing mechanism, it is required to create higher gradients of diffusing components and use the channels of ever smaller cross section.

Initially, the development of microreactor technology proceeded along this path [6,7]. However, with miniaturization of the connecting capillaries, the flow remains laminar, and the reaction zone is absent as unnecessary, since mixing occurs directly behind the junction of capillaries supplying fresh reagents. This approach has its drawbacks: pumping fluid through narrow channels requires the application of significant pressure at the ends of the installation, and the yield of the product decreases. Besides, there is a restriction on the type of reactions that can be implemented on such reactors, since the channel length determines the mixing time [12]. Another approach involves the creation of a special reactor zone, where the convection is organized to mix the species (the advanced-flow microreactor, AFMR) [8]. This leads to an increase in the product yield, and also allows to organize the process for reactions with smaller reaction rate [12]. It should be noted that the development of the AFMR unit requires an individual approach to each reaction and large amount of preliminary theoretical and experimental work, the joint work of different specialists (both chemists and hydrodynamicists). At present, there are several examples of well-developed technologies based on the CFMR/AFMR for the production of pharmaceutical substances by the method of continuous-flow synthesis [9–11,13]. In the last few years, different types of convective micromixers for the AFMR unit have been proposed [13–15]. Furthermore, various techniques have been developed for mixing typically laminar flows in the CFMR. Among them are passive methods, where the mixing effect is introduced by geometry [16] or using bas-relief structures on the bottom of the channel [17] and active methods using an external Braille pin actuator array [18]. Further micromixer working principles are based on fluidic dielectrophoresis [19] or centrifugal action [20]. The literature on continuous-flow microreactors and micromixers is growing exponentially reflecting the interest of researchers in this field.

In this paper, we propose another way of controlling the mass transfer and mixing intensity in a microreactor. We suggest to use a quasi-plane Hele-Shaw (HS) cell with an adjustable gap width serving as the mixing zone in the AFMR unit (Figure 1). In this case, the cell gap could vary both in space and in time due to a special system of actuators attached to the outer wall (or walls if control is carried out symmetrically from both sides) of the HS cell and having the ability to move slightly in the horizontal direction. Thus, the reactor zone would allow for more intensive convective motion. So far, the HS cell with tunable wide boundaries has been rarely considered in the literature since the HS cell was traditionally regarded as a simplified model of a quasi-two-dimensional fluid motion that arises between two parallel plates. So, from a theoretical point of view, the variation of the HS's gap looked like an unnecessary complication of the problem. On the other hand, the precise manufacturing of plates with a slightly deformed and prescribed relief was technically not an easy task. However, at present, due to the appearance of new materials and the development of 3D-printing technology, the technical problems in manufacturing such HS cell are no longer relevant. There are just a few works dealing with non-planar HS cells. Zhao with colleagues studied both experimentally and theoretically the Saffman-Taylor flow in the HS cell with a uniform gradient of the gap [21]. They found a significant effect of the cell wedging on the appearance of secondary instabilities. Viscous fingering in tapered HS cell was studied in [22]. Non-stationary models have been considered in [23,24]. Works on reactive infiltration in a porous medium are also close to the topic considered in this paper, since the flow in a Hele-Shaw cell is similar in its properties to the flow in porous media [25–27]. The reactive-infiltration instability is an important mechanism for pattern development in media with a heterogeneous permeability in geology.

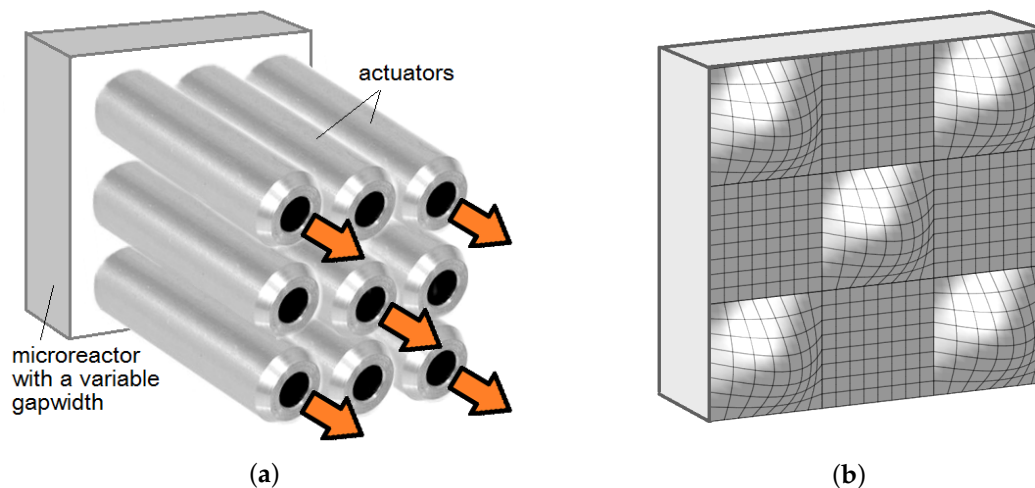


Figure 1. (a) Schematic representation of the method for controlling the local gapwidth of a Hele-show cell using a system of actuators; (b) Deformation of the cell wall, which corresponds to the configuration of the operating actuators shown in (a).

In this paper, we consider the neutralization reaction as a model scheme. Second-order reactions coupled with flows have been attracting the attention of researchers because of their relatively simple but nonlinear kinetics [28–30]. Previously, we have found that convection can arise in the presence of gravity due to the effect of concentration-dependent diffusion (CDD) of species [31–33]. The CDD convection is used here to demonstrate how to control the mass transfer in the microreactor by manipulating its wall relief. The paper is organized as follows: in Section 2 we derive the governing equation for the fluid flow in the HS cell with a variable gap width. In Section 3 we formulate the general mathematical model for the mass transfer in the AFMR unit with the HS cell serving as a mixing zone. The results of the numerical simulations are presented in Section 4. The last section summarizes the highlights of the paper.

2. Mathematical Formulation

We consider a thin cavity defined by $0 \leq x \leq L$, $-d \leq y \leq d$, $-H \leq z \leq H$, where $d \ll L, H$, so that the HS approximation is applied (Figure 2a). For the sake of clarity, suppose that the acceleration due to gravity is directed opposite to z -axis. Assume further that the HS cell gap width can vary both in space and time

$$d(t, x, z) = \pm d_0(1 + \xi(t, x, z)), \quad (1)$$

where $\xi(t, x, z) \ll 1$ is an arbitrary dimensionless function symmetric with respect to the centre of the slot. Thus, the fluid flow in the slot can be approximately considered as quasi-two-dimensional even if the gap between the side walls is adjustable.

By assuming the fluid adhesion to the solid walls, the three-component vector field of the velocity $\mathbf{U}:(U_x, U_y, U_z)$ can be approximated as follows:

$$\begin{aligned} U_x(t, x, y, z) &= \frac{3}{2} \left(1 - \frac{y^2}{d(t, x, z)^2} \right) v_x(t, x, z), \\ U_y(t, x, y, z) &= 0, \\ U_z(t, x, y, z) &= \frac{3}{2} \left(1 - \frac{y^2}{d(t, x, z)^2} \right) v_z(t, x, z), \end{aligned} \quad (2)$$

where $\mathbf{v} = (v_x, v_z)$ is the two-component velocity. The approximations (2) should then be substituted into the Navier-Stokes equation and averaged across the slot

$$\langle \dots \rangle = \frac{1}{2d} \int_{-d}^d \dots dy. \tag{3}$$

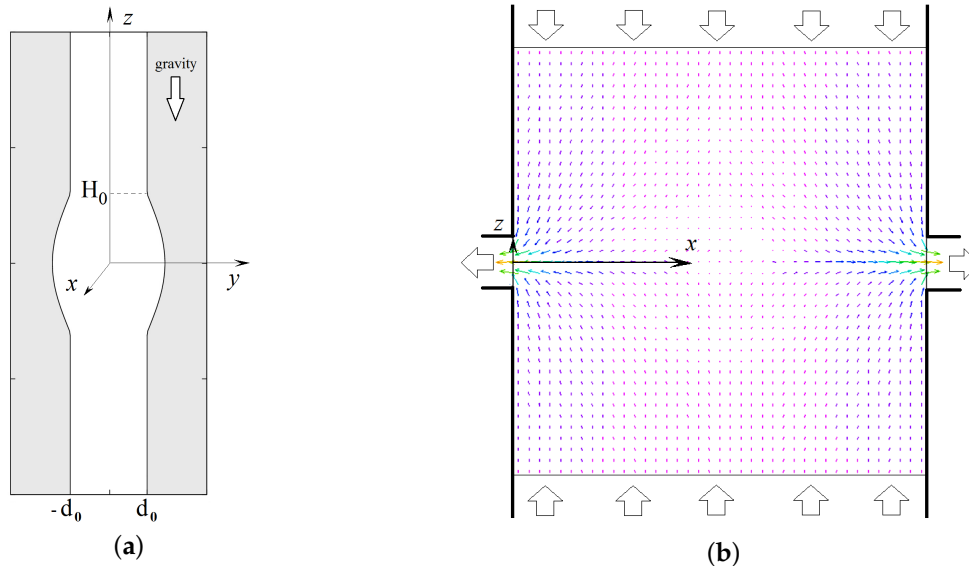


Figure 2. (a) Cross-section of the Hele-Shaw cell with a variable gapwidth and coordinate axes; (b) General scheme for supplying fresh reagents and withdrawing the reaction product in the continuous-flow microreactor. Solutions of acid and base come respectively from above and below, and the reaction product exits through the side channels.

As a result, we obtain the motion equation written in the HS approximation

$$\rho_0 \left(\frac{\partial \mathbf{v}}{\partial t} + \frac{6}{5} \mathbf{v} \cdot \nabla \mathbf{v} \right) = -\nabla p + \eta \Delta \mathbf{v} - \frac{3\eta}{d(t, x, z)^2} \mathbf{v} + \langle \rho \rangle \mathbf{g}, \tag{4}$$

where η is the dynamic viscosity, ρ_0 is the density of the solvent, $\langle \rho \rangle$ is the average medium density, which will be determined below. In addition to the correction factor 6/5 for a nonlinear term, the Equation (4) differs from the standard Navier-Stokes equation by the term proportional to the velocity. This term may be interpreted as the average friction force due to the presence of the plates, and it is analogous to Darcy’s law for the porous medium. In our case, the friction term looks more complicated, since it includes the relief $d(t, x, z)$ of the HS wide walls. Thus, the manipulations with the gap width make it possible to strengthen or weaken locally the friction force acting on the fluid flow.

In this paper, we consider the chemoconvective structures of the characteristic size l . Generally, this quantity is determined rather by the ratio of the reaction rate and the diffusion of the reactants than by the dimensions of the entire cavity, as it happens in the case of thermal convection, which arises due to external heating. To estimate the contribution of different terms, we write Equation (4) in a dimensionless form using l , l^2/D , D/l , and $D\eta/l^2$ as the units of measurement for the length, time, velocity, and pressure, respectively. Here D is the tabular value of the diffusion coefficient of the fastest reagent. Then we get

$$\frac{D\rho_0}{\eta} \left(\frac{\partial \mathbf{v}}{\partial t} + \frac{6}{5} \mathbf{v} \cdot \nabla \mathbf{v} \right) = -\nabla p + \Delta \mathbf{v} - 3 \frac{l^2}{d_0^2 (1 + \xi(t, x, z))^2} \mathbf{v} + \frac{l^3 \mathbf{g}}{\eta D} \langle \rho \rangle, \tag{5}$$

The left-hand side of (5) is multiplied by a dimensionless parameter $1/Sc$, where Sc stands for the Schmidt number. It is mainly used to quantify the relative timescales of viscous momentum transport

and diffusive mass transport. In gases, the Schmidt number is of order of unity, while in the liquids, it is usually very large (about and even more than 1000). Thus, we can neglect the entire left side of the equation in (5). If $l \gg d_0$, then we can neglect the process of the viscous diffusion of the fluid velocity. In the opposite case $l \ll d_0$, the fluid motion becomes so small-scale that the HS approximation (5) is no longer applicable, and the standard Navier-Stokes equation must be used. If the resulting structures are slightly larger or, at least, of the same as the layer thickness, then Equation (5) works well. In what follows, we assume that the condition $l \gg d_0$ is fulfilled throughout the slot, and Equation (5) can be reduced to the Darcy-like equation with a variable permeability of the layer

$$\mathbf{v} = \frac{d(t, x, z)^2}{3\eta} (-\nabla p + \langle \rho \rangle \mathbf{g}), \quad (6)$$

which is given in the dimensional form.

The continuity equation should also be averaged across the slot in the sense of (3). It is convenient to write it in the form of the mass conservation law

$$\frac{\partial}{\partial t} \int_V \langle \rho \rangle dV + \int_V \nabla \cdot (\langle \rho \rangle \mathbf{v}) dV = 0. \quad (7)$$

Since $\langle \rho \rangle$ does not depend on y , the amount of mass is determined only by the volume V . By choosing V in the form of the cylinder, the lateral surface of which is orthogonal to the slot, we can estimate it as $V \approx 2\Sigma d(t, x, z)$, where Σ stands for the area of cylinder's cross-section. Then we obtain

$$\frac{\partial d}{\partial t} + \nabla \cdot (d\mathbf{v}) = 0. \quad (8)$$

Equation (8) implies the effect of weak compressibility of the medium independently of the physical properties of the fluid. Generally, Equations (1), (6) and (8) describe the fluid motion not only in a static situation, when the internal relief of walls is predetermined an apriori, but also in the case of external active control, when the relief is changed in time according to a certain law. The latter effect is taken into account by the first term in (8). It is interesting to note that in the case of the static relief, the governing Equations (6) and (8) coincide with the equations for the filtration of a fluid through a porous medium with variable permeability. If the relief of the side walls does not change in time $d = d(x, z)$, then a simpler formulation is possible. Indeed, instead of Equation (8) we can write

$$\nabla \cdot (d\mathbf{v}) = 0. \quad (9)$$

In this case, no divergence condition is satisfied for the filtration rate $\mathbf{u} = d\mathbf{v}$ commonly used in porous media problems. Equation (9) allows the introduction of the stream function

$$u_x = \frac{\partial \Psi}{\partial z}, \quad u_z = -\frac{\partial \Psi}{\partial x}, \quad (10)$$

and the motion Equation (6) then can be rewritten in the following form:

$$\Delta \Psi - \frac{3}{d} \nabla d \cdot \nabla \Psi = \frac{gd^3}{3\eta} \frac{\partial \langle \rho \rangle}{\partial x}. \quad (11)$$

As a test reaction, we consider the neutralization of acid A by base B at the rate k and resulting in the production of salt S



The reaction enthalpy is about -57 kJ/mol. Although the reaction (12) is exothermic, we have neglected the heat release in this work, since the effective removal of heat from the reactor zone can be organized with the help of highly heat-conducting wide walls of the HS cell. Let us assume the

aqueous solutions of the acid and base be separated in space at the initial moment (acid at the top, base at the bottom). Since the solutions are aqueous, the system is miscible.

In the last years, this simple, irreversible chemical reaction occurring in liquid-liquid miscible systems was extensively studied, to mention but a few [28,29,31–33]. The Rayleigh-Taylor plumes and fingers are commonly observed under gravity when the heavier A overlies the lighter B [28]. Another mechanism breaking the equilibrium was found to be double diffusion instability and diffusive-layer convection [29]. Recently, we have reported a new type of instability, the CDD convection [31–33]. It belongs to the family of double-diffusion phenomena and arises when the diffusion coefficients of species depend on their concentrations. We have shown that the CDD effect can result in the development of a perfectly regular convective pattern [31]. The effect was found primarily for the pair HNO_3/NaOH , but then it was demonstrated also for other systems, for example, HNO_3/KOH , HCl/NaOH [32,33].

The Boussinesq approximation for the convection problems assumes that the density $\langle \rho \rangle$ changes due to heat and/or reagent concentrations are taken into account only in terms depending on gravity (for example, in the last term in Equation (6)). In all other terms, density variations are neglected. Thus, we express the medium density $\langle \rho \rangle$ through the concentrations of reagents dissolved in water

$$\langle \rho \rangle = \rho_0(1 + \beta_A A + \beta_B B + \beta_S S), \quad (13)$$

Here, $\beta_{A,B,S}$ stand for the set of solutal expansion coefficients, respectively.

We scale the problem by using $2d_0$, $4d_0^2/D_{a0}$, $D_{a0}/2d_0$ and A_0 as the units of measurement for the length, time, velocity and concentration, respectively. Here D_{a0} is the tabular value of the diffusion coefficient of acid in water at the temperature of 25 °C and ultra-low concentration. A_0 stands for the initial concentration of acid. Then we obtain the set of equations for species coupled to the Navier-Stokes equation, written in the dimensionless form:

$$\Delta \Psi - \frac{3}{d} \nabla d \cdot \nabla \Psi = \frac{d^3}{12} \left(R_A \frac{\partial A}{\partial x} + R_B \frac{\partial B}{\partial x} + R_S \frac{\partial S}{\partial x} \right), \quad (14)$$

$$\frac{\partial A}{\partial t} + \frac{1}{d} \left(\frac{\partial \Psi}{\partial z} \frac{\partial A}{\partial x} - \frac{\partial A}{\partial x} \frac{\partial \Psi}{\partial z} \right) = \nabla D_a(A) \nabla A - \alpha AB, \quad (15)$$

$$\frac{\partial B}{\partial t} + \frac{1}{d} \left(\frac{\partial \Psi}{\partial z} \frac{\partial B}{\partial x} - \frac{\partial B}{\partial x} \frac{\partial \Psi}{\partial z} \right) = \nabla D_b(B) \nabla B - \alpha AB, \quad (16)$$

$$\frac{\partial S}{\partial t} + \frac{1}{d} \left(\frac{\partial \Psi}{\partial z} \frac{\partial S}{\partial x} - \frac{\partial S}{\partial x} \frac{\partial \Psi}{\partial z} \right) = \nabla D_s(S) \nabla S + \alpha AB. \quad (17)$$

In this paper, we use the concentration-dependent diffusion model developed for the pair HNO_3/NaOH , which works well up to 3 mol/L [31]

$$D_a(A) \approx 0.16A + 0.88,$$

$$D_b(B) \approx -0.09B + 0.59, \quad (18)$$

$$D_s(S) \approx -0.28S + 0.48.$$

The dimensionless parameters which appearing in Equations (14)–(17) are the Damköhler number $\alpha = 4kA_0d_0^2/D_{a0}$, and the set of concentration Rayleigh numbers $R_i = g\beta_i A_0 8d_0^2/\nu D_{a0}$ ($i = a, b, s$). The parameter α is estimated to be about $\alpha = 10^3$. The Rayleigh numbers can be estimated from experimental data as $R_A = 1.5 \times 10^5$, $R_B = 1.8 \times 10^5$, $R_S = 2.4 \times 10^5$ [33].

3. Microreactor Configuration

Let us assume that the acid solution is continuously supplied through the upper boundary, and the base solution is fed through the lower boundary (Figure 2b)

$$\begin{aligned} z = H & : A = 1, B = 0, S = 0, \Psi = Q \frac{x}{L}, \\ z = -H & : A = 0, B = 1, S = 0, \Psi = Q \left(1 - \frac{x}{L}\right), \end{aligned} \quad (19)$$

where Q is the dimensionless feed rate of the reagent solutions through the incoming channels. This is another important parameter of the system.

Let us assume further that the product removal from the reaction zone occurs through the side tubes (Figure 2b). The boundary conditions for the concentrations at the outlets can be specified assuming that the flow in output channels is sufficiently strong to neglect the diffusion transport [34]

$$x = 0, L : \frac{\partial A}{\partial x} = 0, \frac{\partial B}{\partial x} = 0, \frac{\partial S}{\partial x} = 0. \quad (20)$$

To be specific, let us define the wall profile by the following function:

$$d(t, x, z) = 1 + \zeta(t) \mathbf{H}(H_0 - z) \mathbf{H}(H_0 + z) \cos \frac{\pi z}{2H_0}, \quad (21)$$

where \mathbf{H} stands for the Heaviside step function. Equation (21) ensures that gap variation occurs only within the band $-H_0 \leq z \leq H_0$, and the amplitude ζ uniquely determines the deviation of the walls from the planar shape. Figure 2a gives the example of non-planar HS cell for $\zeta = 0.3$. For sidewalls, we specify

$$\begin{aligned} x = 0 & : \Psi = \frac{1}{2} \mathbf{H}(H_0 - z) \mathbf{H}(H_0 + z) Q \left(1 - \frac{z}{H_0}\right) + Q \mathbf{H}(-H_0 - z), \\ x = L & : \Psi = \frac{1}{2} \mathbf{H}(H_0 - z) \mathbf{H}(H_0 + z) Q \left(1 + \frac{z}{H_0}\right) + Q \mathbf{H}(z - H_0). \end{aligned} \quad (22)$$

In order to characterize the nonlinear dynamics resulting from the coupling between chemical reactions and hydrodynamic flows, various types of the integral measurements have been performed during the numerical simulations.

The important measure is given by the reaction rate $R(t)$ computed in terms of the area of the reaction zone, i.e., the number of points where the concentration of salt $S(t, x, z)$ is larger than an arbitrary threshold S^* . In other words, we compute a time-dependent quantity

$$R(t) = \frac{1}{2HL} \int_0^L \int_{-H}^H \mu(x, z) dx dz, \quad (23)$$

where $\mu = 1$ if $S(x, z, t) > S^*$ (S^* is set to be 0.001) and zero otherwise. The integral (23) is normalized by the area of the HS unit. It is normally expected that the rate of reaction should increase because of the fluid convection.

The main control parameter in the problem is the total yield of the reaction product through the output channels. We can estimate it by calculating the instantaneous flux of solvent that removes salt S from the reactor zone through the right and left channels

$$f_S(t) = \left| \int_{left} u_x S dz \right| + \left| \int_{right} u_x S dz \right|. \quad (24)$$

Since the process can be time-periodic or even non-stationary, it makes sense to average the fluid flow (24) over time

$$F_S = \frac{1}{\tau} \int_0^{\tau} f_S(t) dt, \quad (25)$$

where the averaging procedure should be carried out over the entire time τ of the observation so that the quantity F_S becomes the total average yield of the reaction product through the output channels.

The formulated non-stationary boundary value problem (14)–(22) for the variables Ψ , A , B , and S was solved numerically by a finite-difference method. The partial differential equations were approximated by standard finite-difference expressions using one-sided forward differences for time derivatives and central differences for spatial derivatives. The main calculations were carried out on uniform grids with the coordinate step of 0.2. For example, for the reaction zone 100×100 , a square grid of 500×500 nodes was used. As it was shown in [32], such a grid guarantees a sufficiently high resolution for detecting CDD convection.

4. Results of Numerical Simulations

4.1. Batch Microreactor with a Planar HS Cell Unit

Let us first consider the case when the reactor is a closed system. The reagents are preloaded carefully into the HS cell with perfectly planar side walls, then the reactor is closed, and the system evolves without external influence. Thus, here we deal with a typical batch reactor. Equations (14)–(22) are still suitable for numerical simulation of the transfer processes in the BR. However, the influx of fresh reagents and the product outflux must be set to zero: $Q = 0$. In what follows we assume that the initial concentrations of acid and base are equal to the same value A_0 .

Consider first the results for the BR with perfectly planar wide walls: $\zeta = 0$. When the solutions are just brought into contact, then the reaction front slowly expands over time in the non-convective mode according to the root law (Figure 3a, $t < 1.5$). In real terms, one dimensionless unit of time corresponds to 320 s. Under gravity, one then observes the development of the localized cellular chemoconvection (Figure 3a, $t > 1.5$). The instability occurs in a narrow horizontal band adjacent to the original contact surface. The typical distribution of salt concentration is shown in Figure 3b. As it was experimentally shown in [31,32], such a chemo-convective circulation in the BR could continue tens of hours until the moment when the reagents were completely consumed. The mechanism of the instability is as follows. It may occur when an emerging component starts to accumulate near the reaction front. If its molecules quickly leave the reaction zone, then it has no significant influence on the instability scenario. But if the diffusion coefficient of the reaction product decreases with the growth of its concentration (concentration-dependent diffusion effect, CDD), it can progressively make a local minimum in the density profile (figuratively, “density pocket”). Figure 3a shows that the occurrence of the CDD instability significantly increases the reaction rate $R(t)$ at $t > 1.5$ since the fluid layers begin to mix due to convection.

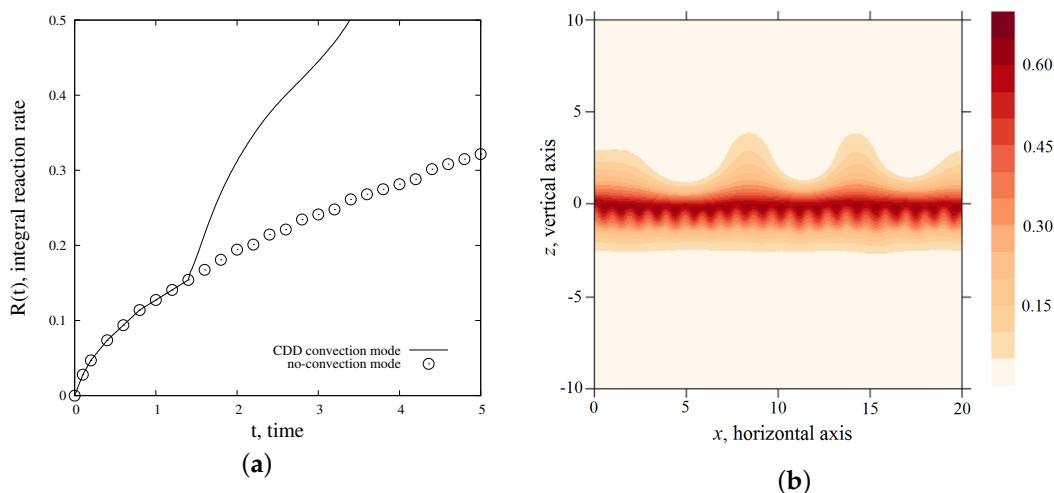


Figure 3. (a) Evolution of the reaction rate $R(t)$ for the batch reactor with perfectly planar Hele-Shaw unit working in either the pure reaction-diffusion mode (open circles) or the concentration-dependent diffusion (CDD) convection mode (solid line); (b) Salt concentration field at time $t = 3$ for the same reactor.

4.2. Continuous-Flow Microreactor with a Prescribed Non-Planar Wall Relief

Consider now the results for the open reacting system. As an example of the CFMR, we will consider the HS cell with non-planar wide walls described by formula (21). The vertical cross-section of this microreactor is shown in Figure 2a. We assume here that the shape of the walls of the reactor does not change in time: $\zeta = \text{const}$. The relief of the reactor walls is designed in such a way that the thickening of the gap between the walls of the microreactor occurs just in the zone, where the reaction-diffusion-convection processes act jointly. Let us consider the behavior of the two microreactors with a larger (100×100) and smaller (20×20) HS unit.

Figure 4a shows the yield of the reaction for a larger microreactor (100×100). The figure presents the dependence of the product output F_S on the amplitude ζ , which defines the deviation of the sidewalls of the HS cell from the planar shape. It is seen that the gradual expansion of the reaction zone due to the local increase in the HS cell gap leads to more intensive mixing and an increase in the yield of the product according to a linear law (Figure 4a, $0 < \zeta < 0.5$). The trend continues up to about $\zeta \approx 0.5$, and then the system goes to saturation: the further expansion of the zone does not affect the quantity of the reaction product. Quite a similar dependence is demonstrated by the percentage of the reaction product in the total flux exiting the reactor: it also increases linearly with ζ , reaches the maximum value of 27.5% at $\zeta = 0.6$, and then even slightly decreases. Thus, one can conclude that by manipulating the gap width it is possible to increase the integral average flux of the product by a factor of 2.

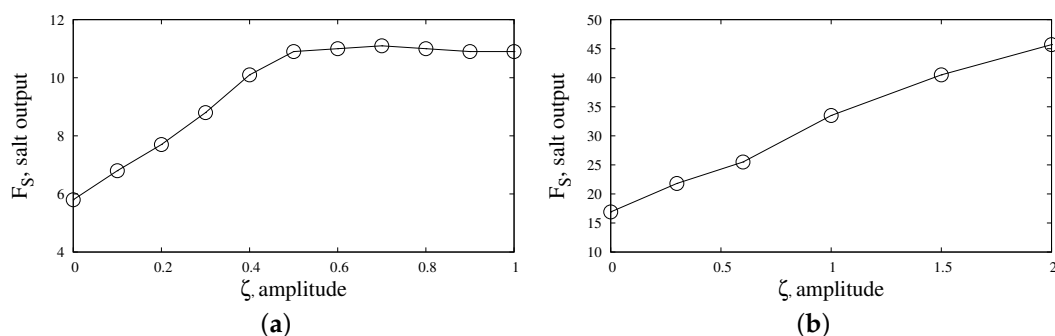


Figure 4. The average flow of the reaction product at the outlet of the continuous-flow reactor as a function of the amplitude ζ : (a) large Hele-Shaw (HS) unit (100×100); (b) small HS unit (20×20). $H_0 = 1$, $Q = 100$.

Numerical modeling has shown that the process is not stationary. An unsteady flow occurs when the reagent concentration is depleted and the products of reaction are pumped out resulting in the formation of the low-density zone. This zone floats up under the action of the Archimedes force and thus disrupts the continuity of the acid supply. The secondary instability in the form of pop-up plumes, which carry away salt, reduces the overall efficiency of the microreactor. Therefore, strong pulsations of concentration fields are observed at the exit of the reactor, especially in the beginning of evolution.

Let us now consider the operation of the AFMR with a smaller reactor zone of 20×20 units, but keeping the characteristic size of the chemoconvective cells (it is defined by the basic value of the gap width). Figure 4b shows that the integral flux of the reaction product in such a microreactor also increases significantly. The reason is that the HS cell becomes smaller with the same intensity of convective motion determined by the nature of the instability, which leads to better mixing in the system, and, therefore, to an increase in the spatial reaction rate. It is interesting to note that the effect of an increase in the product yield with the expansion of the convection zone is observed in the entire range of the amplitude ζ . Finally, a twofold increase in the amplitude ζ results in an almost three-fold increase in the integral product yield. Probably, it is possible to increase the amplitude ζ further, but a question arises about the validity of the mathematical model obtained for the small gap variations ($\zeta \ll d_0$). Another parameter affecting the efficiency of the microreactor is the width of the band H_0 , over which the gap slot is varied.

Simulations have shown that in the smaller reactor the flow becomes more stable. At the outlets, the fluid flows experience weak pulsations, which are associated with the spatially periodic nature of the CDD instability. When the solution with the product is sucked out from the HS cell, the convective cells that are rich in salt leave the reactor one after the other resulting in a periodic behavior of the product flow. We found that a significant contribution to the overall stabilization of the transfer processes in the microreactor is made by the continuous outflows from the reactor zone.

4.3. Continuous-Flow Microreactor with a Wall Relief Changing in Time

Suppose now that the walls are made of a flexible, but chemically inert material that allows changing the wall profile in time. Micron changes in the shape of the walls pose serious requirements for the controller design, but it opens up a broad potential for controlling mass transfer in the CFMR. Figures 5 and 6 illustrate these new capabilities. Figure 5 shows the salt concentration field for three consecutive times, which correspond to three different wall profiles. Evolution begins when the walls are slightly curved outward ($H_0 = 10$, $\zeta = 0.5$, Figure 5a). At that time, the permeability of the reactor zone is maximal, the convection develops vigorously capturing the entire volume of the reactor (Figure 6, $t < 0.05$), and the highest product yield is observed. At $t = 0.05$, the wide walls have been quickly rearranged in such a way that the region remains convex only within the band $-5 \leq z \leq 5$ ($H_0 = 5$, $\zeta = 0.5$). The permeability at the microreactor periphery decreases and the convection attenuates there remaining only within the specified band (Figure 5b). At the outlets, the fluid flows

experience pulsations, which are associated with the spatially periodic nature of the CDD instability (Figure 6, $0.05 < t < 1$). Rich in salt convective cells eventually leave the microreactor one after the other resulting in a periodic behavior. Finally, one can even completely suppress convection by specifying a slightly concave shape ($H_0 = 5$, $\zeta = -0.5$) for the walls (Figure 5c). This is clearly seen in the stabilization of the product yield at a lower level (Figure 6, $t > 1$).

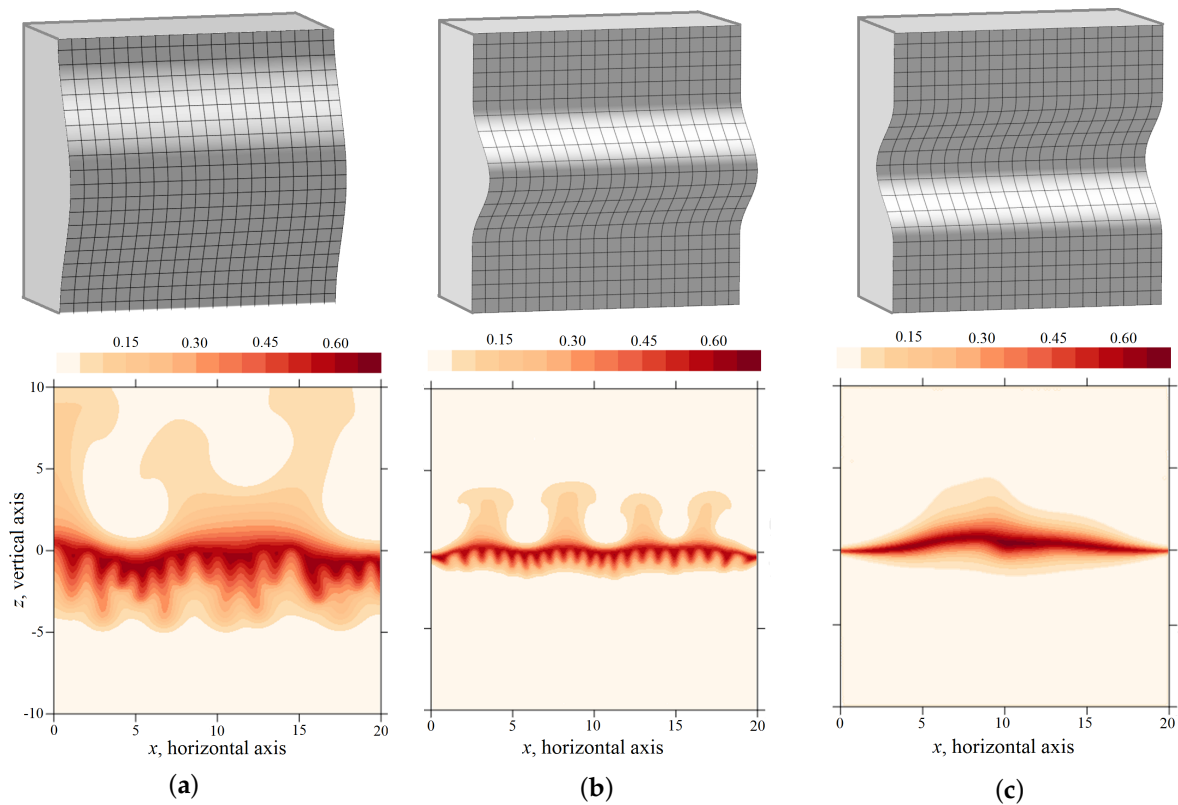


Figure 5. Evolution of the salt concentration (lower row) in a continuous-flow reactor real-time controlled by the deviations of the wide walls from the perfectly planar form (upper row). The frames (a–c) from left to right correspond to times $t = 0.05, 0.5, 2$ respectively.

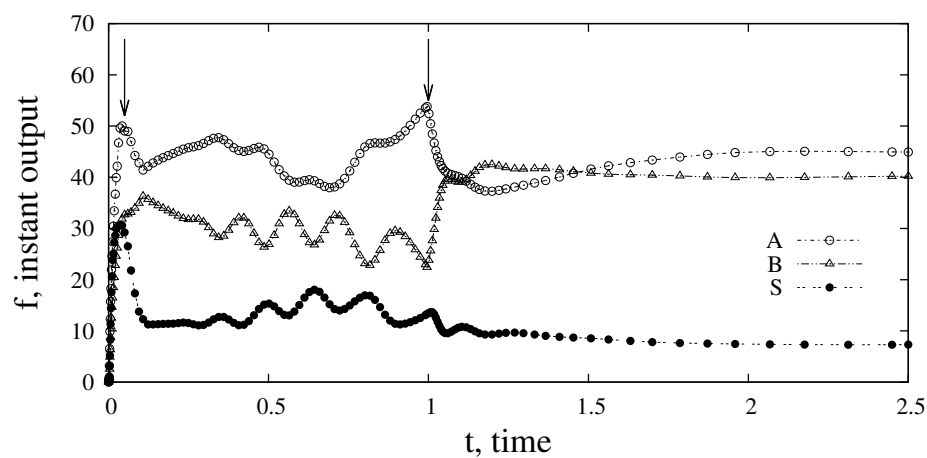


Figure 6. Output from a continuous-flow reactor with walls being tuned in real-time. The time intervals $[0, 0.05]$, $[0.05, 1]$ and $[1, 2.5]$ correspond to the three Hele-Shaw cell configurations shown in Figure 5, respectively. Switches between configurations are indicated by arrows.

5. Discussion and Conclusions

The theory and practice of the continuous-flow microreactors, which use hydrodynamic or convective motions of fluid for mixing reagents, are being actively developed for chemical technologies of pharmaceutical production. The production of the pharmaceutical substances requires flexibility in reconfiguring the production line and the continuity of its operation. Besides, the pharmaceutical production usually consists of a large number of intermediate stages, continuously flowing one into another, which is difficult to achieve in the framework of a traditional batch reactor. Being developed quite recently, the continuous-flow microreactors have already demonstrated their efficiency compared to their counterparts.

In this paper, we theoretically consider the influence of the shape of the microreactor walls on the mass transfer processes inside it. To be more precise, we consider the Hele-Shaw cell, which is externally controlled by the system of actuators enabling the variation of the width of the cell gap in both time and space. Our paper shows that such manipulations open up broad possibilities for controlling the processes inside the reactor. Such control can be organized in various ways. For example, the control can be organized passively by pre-prototyping the shape of the reactor walls to maintain certain flow patterns. In this case, the shape of the wall profile can be computed and tested. For instance, the intensity of an undesirable flow can be significantly reduced by setting a narrower gap between the sidewalls of the reactor, i.e., by reducing the local permeability of the medium. In the opposite case of the flow, that has a useful effect in the microreactor, it can be supported by expanding locally the gap in the area where this flow is present. To apply active control, the walls of the microreactor must be deformable. Then one has to establish a real-time feedback between the actuators and sensors signaling the mass transfer processes inside the reactor. If the product yield is taken as a control parameter, then the controller could be programmed so that it would stimulate useful convective structure in real time.

In conclusion, in this paper, we have studied the effect of the wall shape changes on mass transfer in the CFMR reactor. This method to control the microreactor has not yet been discussed in the literature, since, until the invention of 3D-printing, the fabrication of microcells with slightly non-planar walls was not a trivial task. To implement it, the walls of the microreactor must be made of a deformable, chemically inert and resistant material. If this condition is fulfilled, then it is possible to design a device that would change the local permeability of the quasi-planar microreactor in real-time. We have shown that manipulations of the wall shape open up broad possibilities for controlling the processes in the reactor.

Author Contributions: Conceptualization, D.B.; Numerical simulations, R.S.; Writing and Draft Preparation, D.B. and R.S. All authors have read and agreed to the published version of the manuscript.

Funding: The reported study was funded by Russian Foundation for Basic Research and Ministry of Science and Education of Perm region (No. 17-41-590100).

Conflicts of Interest: The authors declare no conflict of interest.

References

1. Levich, V.G. *Physicochemical Hydrodynamics*; Prentice-Hall: Englewood Cliffs, NJ, USA, 1962; 700p.
2. Levich, V.G.; Brodskii, A.M.; Pismen, L.M. A contribution to theory of branching homogeneous chain reaction in a flow. *Dokl. Akad. Nauk SSSR* **1967**, *176*, 371–373.
3. Jakobsen, H.A. *Chemical Reactor Modeling. Multiphase Reactive Flows*; Springer-Verlag: Berlin/Heidelberg, Germany, 2008; 1238p.
4. Levenspiel, O. *Chemical Reaction Engineering*; Wiley: New York, NY, USA, 1999; 578p.
5. Reschetilowski, W. (Ed.) *Microreactors in Preparative Chemistry*; Wiley-VCH: Weinheim, Germany, 2013; 352p.
6. Hessel, V.L.; Holger-Schonfeld, F. Micromixers—A review on passive and active mixing principles. *Chem. Eng. Sci.* **2005**, *60*, 2479–2501. [[CrossRef](#)]
7. Jensen, K.F. Microreaction engineering—Is small better? *Chem. Eng. Sci.* **2001**, *56*, 293–303. [[CrossRef](#)]
8. Nieves-Remacha, M.J.; Kulkarni, A.A.; Jensen, K.F. Hydrodynamics of liquid-liquid dispersion in an Advanced-Flow Reactor. *Ind. Eng. Chem. Res.* **2012**, *51*, 16251–16262. [[CrossRef](#)]

9. Filipponi, P.; Ostacolo, C.; Novellino, E.; Pellicciari, R.; Gioiello, A. Continuous Flow Synthesis of Thieno[2,3-c]isoquinolin-5(4H)-one Scaffold: A Valuable Source of PARP-1 Inhibitors. *Org. Process Res. Dev.* **2014**, *18*, 1345–1353. [[CrossRef](#)]
10. Baumann, M.; Baxendale, I.R. The synthesis of active pharmaceutical ingredients (APIs) using continuous flow chemistry. *Beilstein J. Org. Chem.* **2015**, *52*, 1194–1219. [[CrossRef](#)]
11. Pellegatti, L.; Sedelmeier, J. Synthesis of Vildagliptin Utilizing Continuous Flow and Batch Technologies. *Org. Process Res. Dev.* **2015**, *19*, 551–554. [[CrossRef](#)]
12. Wegner, J.; Ceylan, S.; Kirschning, A. Ten key issues in modern flow chemistry. *Chem. Commun.* **2011**, *47*, 4583–4592. [[CrossRef](#)]
13. Mascia, S.; Heider, P.L.; Zhang, H.; Lakerveld, R.; Benyahia, B.; Barton, P.I.; Braatz, R.D.; Cooney, C.L.; Evans, J.M.B.; Jamison, T.F.; et al. End-to-end continuous manufacturing of pharmaceuticals: integrated synthesis, purification, and final dosage formation. *Angew. Chem. Int. Ed.* **2013**, *52*, 12359–12363. [[CrossRef](#)]
14. Ju, J.; Warrick, J. Passive micromixer using by convection and surface tension effects with air–liquid interface. *BioChip J.* **2013**, *7*, 361–366. [[CrossRef](#)]
15. Bratsun, D.; Kostarev, K.; Mizev, A.; Aland, S.; Mokbel, M.; Schwarzenberger, K.; Eckert, K. Adaptive micromixer based on the solutocapillary Marangoni effect in a continuous–flow microreactor. *Micromachines* **2018**, *9*, 600. [[CrossRef](#)] [[PubMed](#)]
16. Cheng, W.L.; Erbay, C.V.; Sadr, R.; Han, H. Dynamic Flow Characteristics and Design Principles of Laminar Flow Microbial Fuel Cells. *Micromachines* **2018**, *9*, 479. [[CrossRef](#)] [[PubMed](#)]
17. Stroock, A.D.; Dertinger, S.K.W.; Ajdari, A.; Mezic, I.; Stone, H.A.; Whitesides, G.M. Chaotic Mixer for Microchannels. *Science* **2002**, *295*, 647–651. [[CrossRef](#)] [[PubMed](#)]
18. Abbas, Y.; Miwa, J.; Zengerle, R.; von Stetten, F. Active Continuous-Flow Micromixer Using an External Braille Pin Actuator Array. *Micromachines* **2013**, *4*, 80–89. [[CrossRef](#)]
19. Mavrogiannis, N.; Desmond, M.; Ling, K.; Fu, X.; Gagnon, Z. Microfluidic Mixing and Analog On-Chip Concentration Control Using Fluidic Dielectrophoresis. *Micromachines* **2016**, *7*, 214. [[CrossRef](#)]
20. Cai, Z.; Xiang, J.; Chen, H.; Wang, W. A Rapid Micromixer for Centrifugal Microfluidic Platforms. *Micromachines* **2016**, *7*, 89. [[CrossRef](#)]
21. Zhao, H.; Casademunt, J.; Yeung, C.; Maher, J.V. Perturbing Hele-Shaw flow with a small gap gradient. *Phys. Rev. A* **1992**, *45*, 2455–2460. [[CrossRef](#)]
22. Al-Housseiny, T.T.; Stone, H.A. Controlling viscous fingering in tapered Hele-Shaw cells. *Phys. Fluids* **2013**, *25*, 092102. [[CrossRef](#)]
23. Zhang, S.-Z.; Louis, E.; Pla, O.; Guinea, F. Linear stability analysis of the Hele-Shaw cell with lifting plates. *Eur. Phys. J. B* **1998**, *1*, 123–127. [[CrossRef](#)]
24. Dias, E.O.; Miranda, J.A. Taper-induced control of viscous fingering in variable-gap Hele-Shaw flows. *Phys. Rev. E* **2013**, *87*, 053015. [[CrossRef](#)]
25. Chadam, J.; Hoff, D.; Merino, E.; Ortoleva, P.; Sen, A. Reactive Infiltration Instabilities. *IMA J. Appl. Math.* **1986**, *36*, 207–221. [[CrossRef](#)]
26. Ortoleva, P.; Chadam, J.; Merino, E.; Sen, A. Geochemical self-organization II: The reactive-infiltration instability. *Am. J. Sci.* **1987**, *287*, 1008–1040. [[CrossRef](#)]
27. Ortoleva, P.J. *Geochemical Self-Organization*; Oxford University Press: Oxford, UK, 1994; 426p.
28. Almarcha, C.; Trevelyan, P.M.J.; Grosfils, P.; De Wit, A. Chemically Driven Hydrodynamic Instabilities. *Phys. Rev. Lett.* **2010**, *104*, 044501. [[CrossRef](#)] [[PubMed](#)]
29. Trevelyan, P.M.J.; Almarcha, C.; De Wit, A. Buoyancy-driven instabilities around miscible $A + B \rightarrow C$ reaction fronts: a general classification. *Phys. Rev. E* **2015**, *91*, 023001. [[CrossRef](#)]
30. Hejazi, S.H.; Trevelyan, P.M.J.; Azaiez, J.; De Wit, A. Viscous fingering of a miscible reactive $A + B \rightarrow C$ interface: a linear stability analysis. *J. Fluid Mech.* **2010**, *652*, 501–528. [[CrossRef](#)]
31. Bratsun, D.; Kostarev, K.; Mizev, A.; Mosheva, E. Concentration-dependent diffusion instability in reactive miscible fluids. *Phys. Rev. E* **2015**, *92*, 011003. [[CrossRef](#)]
32. Bratsun, D.A.; Stepkina, O.S.; Kostarev, K.G.; Mizev, A.I.; Mosheva, E.A. Development of Concentration-Dependent Diffusion Instability in Reactive Miscible Fluids Under Influence of Constant or Variable Inertia. *Microgravity Sci. Technol.* **2016**, *28*, 575–585. [[CrossRef](#)]

33. Bratsun, D.; Mizev, A.; Mosheva, E.; Kostarev, K. Shock-wave-like structures induced by an exothermic neutralization reaction in miscible fluids. *Phys. Rev. E* **2017**, *96*, 053106. [[CrossRef](#)]
34. Danckwerts, P.V. *Gas-Liquid Reactions*; McGraw-Hill Book Co.: New York, NY, USA, 1970; 276p.



© 2019 by the authors. Licensee MDPI, Basel, Switzerland. This article is an open access article distributed under the terms and conditions of the Creative Commons Attribution (CC BY) license (<http://creativecommons.org/licenses/by/4.0/>).